# Made-to-Order Heterostructured Nanoparticle Libraries

Raymond E. Schaak,[1,2,3,*] Benjamin C. Steimle,[1] and Julie L. Fenton[1]

[1] *Department of Chemistry,* [2] *Department of Chemical Engineering, and* [3] *Materials Research Institute, The Pennsylvania State University, University Park, PA 16802*

**Corresponding author:**
* res20@psu.edu

**Website:** https://sites.psu.edu/rayschaak

**Twitter:**
- Raymond Schaak: @rayschaak
- Benjamin Steimle: @BCSteimle
- Julie Fenton: @julielfenton

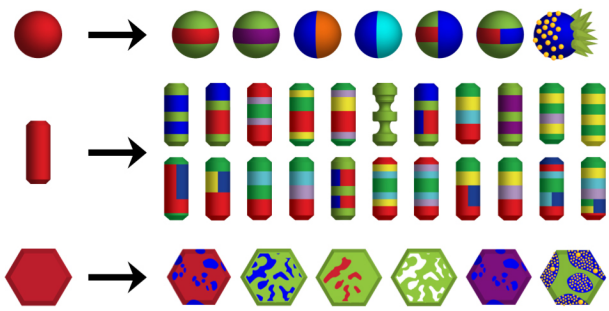

**CONSPECTUS:**

Nanoparticles that contain multiple materials connected through interfaces, often referred to as heterostructured nanoparticles, are important constructs for many current and emerging applications. Such particles combine semiconductors, metals, insulators, catalysts, magnets, and other functional components that interact synergistically to enable applications in areas that include energy, nanomedicine, nanophotonics, photocatalysis, and active matter. To synthesize heterostructured nanoparticles, it is important to control all of the property-defining features of individual nanoparticles – size, shape, uniformity, crystal structure, composition, surface chemistry, dispersibility – in addition to interfaces, asymmetry, and spatial organization, which facilitate communication among the constituent materials and enable their synergistic functions. While it is challenging to control all of these nanoscale features simultaneously, nanoparticle cation exchange reactions offer powerful capabilities that overcome many of the synthetic bottlenecks. In these reactions, which are often carried out on metal chalcogenide materials such as roxbyite copper sulfide ($Cu_{1.8}S$) that have high cation mobilities and a high density of vacancies, cations from solution replace cations in the nanoparticle. Replacing only a fraction of the cations can produce phase-segregated products having internal interfaces, *i.e.*

heterostructured nanoparticles. By carrying out multiple partial cation exchange reactions, multicomponent heterostructured nanoparticles can be synthesized.

In this Account, we discuss the use of multiple sequential partial cation exchange reactions to rationally construct complex heterostructured nanoparticles, toward the goal of made-to-order synthesis. Sequential partial exchange of the $Cu^+$ cations in roxbyite $Cu_{1.8}S$ spheres, rods, and plates produces a library of 47 derivatives that maintain the size, shape, and uniformity defined by the roxbyite templates while introducing various types of interfaces and different materials into the resulting heterostructured nanoparticles. Using an excess of metal salt reagents, reaction time controls the extent of partial cation exchange. By instead using substoichiometric metal salt reagents, the extent of partial cation exchange can be precisely controlled by cation concentration. This approach allows significant control over the number, order, and location of partial cation exchange reactions. Up to 7 sequential partial cation exchange reactions can be applied to roxbyite $Cu_{1.8}S$ nanorods to produce derivative heterostructured nanorods containing as many as 6 different materials, 8 internal interfaces, and 11 segments, *i.e.* ZnS–$CuInS_2$–$CuGaS_2$–CoS–[CdS–(ZnS–$CuInS_2$)]–$Cu_{1.8}S$. We considered all possible injection sequences of five cations ($Zn^{2+}$, $Cd^{2+}$, $Co^{2+}$, $In^{3+}$, $Ga^{3+}$) applied to all accessible $Cu_{1.8}S$-derived nanorod precursors, along with simple design criteria based on preferred cation exchange locations and crystal structure relationships. Using these guidelines, we mapped out synthetically feasible pathways to 65,520 distinct heterostructured nanorods, experimentally observed 113 members of this heterostructured nanorod megalibrary, and then made three of these with high yield and in isolatable quantities. By expanding these capabilities into a broader scope of materials and identifying additional design guidelines, it should be possible to move beyond model systems and access functional targets rationally and retrosynthetically. Overall, the ability to access large libraries of complex heterostructured nanoparticles in a made-to-order manner is an important step toward bridging the gap between design and synthesis.

## KEY REFERENCES


- Fenton, J. L.; Steimle, B. C.; Schaak, R. E. Tunable Intraparticle Frameworks for Creating Complex Heterostructured Nanoparticles Libraries. *Science* **2018**, *360*, 513-517.[1] *We developed the synthetic methodology that uses cation exchange transformations, chemoselective etching, and regioselective deposition to sequentially modify copper sulfide nanoparticles, producing a library of 47 distinct heterostructured nanoparticle products.*

- Fenton, J. L.; Steimle, B. C.; Schaak, R. E. Exploiting Crystallographic Regioselectivity To Engineer Asymmetric Three-Component Colloidal Nanoparticle Isomers Using Partial Cation Exchange Reactions. *J. Am. Chem. Soc.* **2018**, *140*, 6771-6775.[2] *Crystal structure relationships directly impact the direction of cation exchange and the orientation of interfaces within heterostructured metal sulfide nanoparticles produced using partial cation exchange reactions. We applied this concept of crystallographic regioselectivity to generated five distinct nanoparticle isomers containing various combinations of $Cu_{1.8}S$, ZnS, and CdS*.

- Steimle, B. C.; Fenton, J. L.; Schaak, R. E. Rational Construction of a Scalable Heterostructured Nanorod Megalibrary. *Science* **2020**, 367, 418-424.[3] *Application of up to seven sequential partial cation exchange reactions using five different cations in various combinations transforms copper sulfide nanorods into a megalibrary of heterostructured derivatives. We defined synthetically feasible pathways to 65,520*

*distinct heterostructures, experimentally observed 113 unique members of the megalibrary, and synthesized three in scalable quantities.*

## 1. Introduction

Colloidal inorganic nanoparticles are mainstream materials with useful functions. To list just two, color-tunable quantum dots are used in full-color displays[4] and gold nanoparticles are used in photothermal therapy to treat cancer.[5,6] When nanoparticles with useful properties are combined into larger assemblies, they can function synergistically and cooperatively. For example, CdSe, In/Ag, Ag, and $Al_2O_3$ nanoparticles can be assembled together to function as the channel, source/drain, gate, and insulator, respectively, of an all-inorganic-nanoparticle transistor.[7] Nanoparticles can also be combined into other nanoparticles, for example by making discrete nanoparticles that contain two or more materials interfaced together.[8–11] Consider a hypothetical heterostructured nanoparticle that contains a central light-absorbing semiconductor, a water reduction catalyst on one end, and a water oxidation catalyst on the other end, *i.e.* a $catalyst_{red}$–semiconductor–$catalyst_{ox}$ triad.[12,13] This combination of materials, within one nanoscale construct that has interfaces to facilitate charge transfer, is precisely designed to enable light-driven overall water splitting. Similar types of heterostructured nanoparticles containing different materials are central to other applications, including in energy,[12–14] nanomedicine,[15] nanophotonics,[16,17] and active matter.[18,19]

In these and other examples, functional nanomaterials are integrated through solid-solid interfaces that facilitate electronic communication, magnetic coupling, and/or electron transfer. Most are asymmetric, which enables electron-hole separation and directional charge transfer, and precise spatial organization is required to realize the targeted function. For example, if the components of the construct mentioned above were re-arranged to $catalyst_{ox}$–$catalyst_{red}$–semiconductor, overall water splitting could not be achieved because there would be no interface by which electrons could transfer from the semiconductor to the oxidation catalyst. For heterostructured nanoparticles, it is therefore important to control the property-defining features that matter for individual nanoparticles – size, shape, uniformity, crystal structure, composition, surface chemistry, dispersibility – as well as the features that enable synergistic interactions – interfaces, asymmetry, and spatial organization.[9] Synthetic control over all of these features simultaneously is imperative, but this is a formidable challenge with many bottlenecks.

Synthesizing nanoparticles in solution requires soluble reagents dissolved in an appropriate solvent and a chemical or thermal trigger for nucleation, such as decomposition, ligand dissociation, or reduction.[20–23] Subsequent growth is mediated by surface stabilizers, which modulate overall and/or facet-selective growth to influence size, uniformity, morphology, crystal structure, and composition.[24–26] Many reaction parameters influence these characteristics of the product nanoparticles, including (but not limited to) temperature, ramp rate, dwell time, stir rate, atmosphere, heat source, reagent purities, and order and rate of addition of reagents. Given this wide parameter space, these key features can be challenging to control simultaneously even for single-component nanoparticles. Nanoparticles having multiple materials interfaced together asymmetrically with precise spatial organization become even more challenging to synthesize.

Several synthetic approaches are being developed to achieve these goals. These include solution-based growth of one particle on another,[8–11,27,28] substrate-bound growth through chemical or physical vapor deposition,[29] electrodeposition in templates,[30] and chemical deposition in surface-confined nanoreactors.[31,32] These methods are additive, i.e. they involve the growth of one material off of another (called a “seed” particle), building a heterostructured

nanoparticle outward from a seed or surface. Alternatively, chemical transformation reactions can modify the seed particle itself, building interfaces, asymmetry, and multiple materials internally within the seed particle.[33–37]

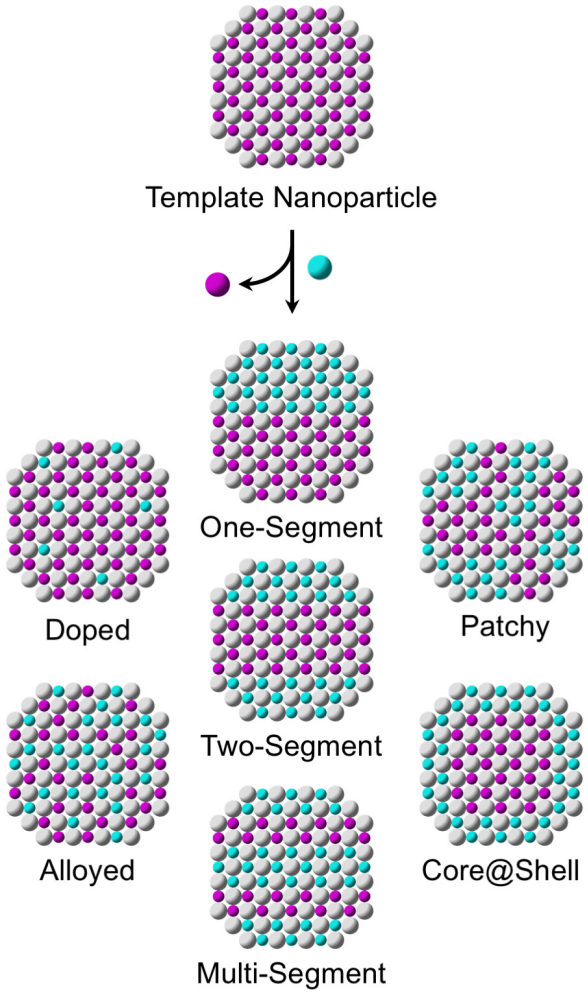


**Figure 1.** Diversity of products accessible using partial cation exchange of a template nanoparticle.

Nanoparticle cation exchange has emerged as a powerful postsynthetic transformation strategy that is capable of achieving many of the aforementioned goals.[37–40] These reactions replace cations in a nanoparticle with cations from solution and are driven thermodynamically through solvation energies, hard-soft acid-base interactions, lattice energies, and solubility constants.[37,41–43] Short diffusion distances afforded by the nanoscale dimensions and cation vacancies in the template nanocrystals that facilitate diffusion help the reactions to occur rapidly.[37,44–46] Cation exchange reactions are often topotactic with size, shape, and crystal structure features maintained even after multiple sequential exchange reactions.[47,48] By arresting these reactions prior to completion, a variety of products can be obtained, including doped, alloyed, and phase-segregated particles that include patchy, core@shell, and heterostructured architectures (Figure 1).[37,49] In this Account, we discuss the development and application of multiple sequential partial cation exchange reactions to produce complex heterostructured nanoparticles and their derivatives.[1–3] Our focus is on the synthetic design

principles that underpin these reactions, as well as the scope of current capabilities. Finally, we describe the integration of sequential partial cation exchange with seeded growth and chemical etching to further expand design capabilities for achieving made-to-order complex nanoparticles.

## 2. Partial Cation Exchange Reactions

Roxbyite copper sulfide, $Cu_{1.8}S$, contains highly mobile $Cu^+$ cations and a high concentration of vacancies,[50] making it particularly useful for nanoparticle cation exchange and a versatile template for these reactions.[1–3,51] Exchanging the $Cu^+$ cations in roxbyite spheres, rods, and platelets with $Zn^{2+}$ and $Cd^{2+}$, where the extent of cation exchange is controlled by reaction time, provides interesting insights into the scope of partial cation exchange behavior (Figure 2).[1] Partial cation exchange of roxbyite spheres with $Zn^{2+}$ produced ZnS–$Cu_{1.8}S$–ZnS sandwich spheres, as had been reported previously.[52] In contrast, $Cd^{2+}$ exchange of the same roxbyite spheres produced Janus spheres, with one hemisphere containing CdS and the other containing $Cu_{1.8}S$.[1] When roxbyite nanorods were used instead of spherical particles, $Zn^{2+}$ exchange introduced multiple ZnS bands, forming either ZnS–$Cu_{1.8}S$–ZnS dual-capped nanorods or ZnS–$Cu_{1.8}S$–ZnS–$Cu_{1.8}S$–ZnS striped nanorods.[1] When roxbyite nanoplates were used, $Zn^{2+}$ exchange produced marbled ZnS filaments in $Cu_{1.8}S$ while $Cd^{2+}$ exchange produced large patches of CdS in $Cu_{1.8}S$.[1] Collectively, cation exchange of $Zn^{2+}$ and $Cd^{2+}$ on "first generation" (G-1) roxbyite spheres, rods, and plates introduced a diverse range of intraparticle frameworks into "second-generation" (G-2) ZnS/$Cu_{1.8}S$ and CdS/$Cu_{1.8}S$ derivatives while maintaining the size, shape, and uniformity of the G-1 templates.[1]

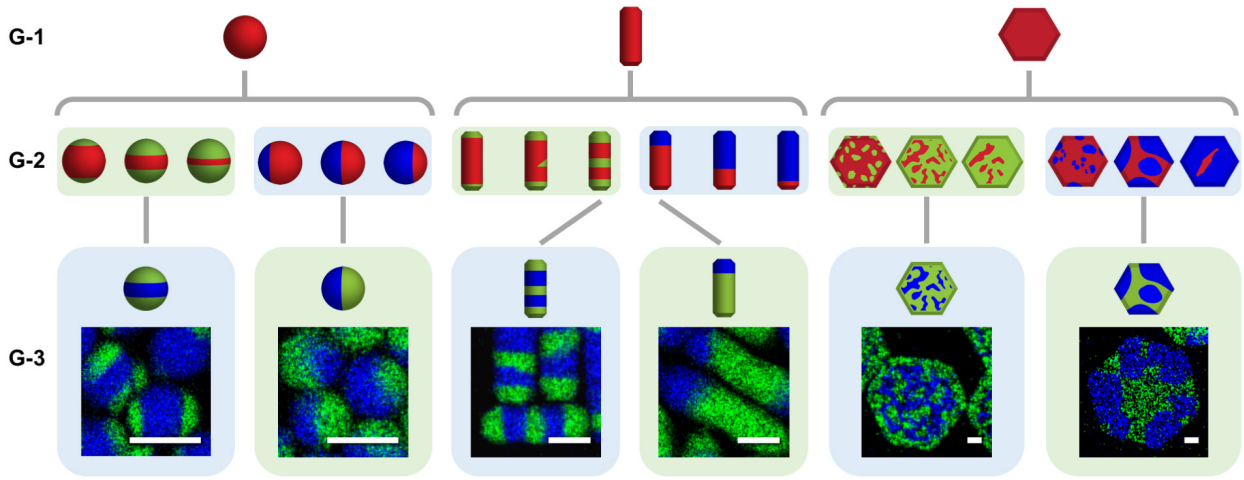


**Figure 2.** First-generation (G-1) roxbyite $Cu_{1.8}S$ spheres, rods, and plates transform to G-2 derivatives upon partial cation exchange with $Zn^{2+}$ or $Cd^{2+}$. In the G-2 ZnS/$Cu_{1.8}S$ and CdS/$Cu_{1.8}S$ particles, the interfaces generally depend on crystallographic relationships and the extent of exchange is controlled by reaction time. One of each G-2 system is used as an example to transform to a derivative G-3 system; both drawings and STEM-EDS element maps are shown. Red = $Cu_{1.8}S$, green = ZnS, blue = CdS. Scale bars are 20 nm. The STEM-EDS maps were adapted with permission from ref. 1, copyright 2018 American Association for the Advancement of Science.

In all of the G-2 samples, the regions of residual roxbyite are amenable to further cation exchange (Figure 2).[1] For the G-2 samples where $Zn^{2+}$ was used during first exchange, $Cd^{2+}$ was used for a subsequent exchange. Similarly, where $Cd^{2+}$ was used during the first exchange, $Zn^{2+}$ was used for a subsequent exchange. This process produced six distinct G-3 CdS/ZnS isomers that maintained the shape and size of the G-1 particles and the intraparticle frameworks of the G-2 particles, but with different sulfide materials. It is also possible to exchange the $Cu^{+}$ in roxbyite with other cations, including $Co^{2+}$, $Mn^{2+}$, and $Ni^{2+}$, which expands the accessible G-3 heterostructured nanoparticles to include CoS, MnS, and $Ni_9S_8$ segments, respectively. All together, the roxbyite spheres, rods, and plates were transformed through partial cation exchange into a library of 47 distinct derivative heterostructured nanoparticles, many with previously unachievable complexity.[1]

### 3. Crystallographic Regioselectivity

Returning to the G-1–to–G-2 transformation in Figure 2, it is useful to understand more about how the $Zn^{2+}$ and $Cd^{2+}$ exchange reactions with roxbyite are different. Recall that, for the roxbyite spheres, exchanging the $Cu^{+}$ cations with $Zn^{2+}$ produced ZnS–$Cu_{1.8}S$–ZnS sandwich spheres, while analogous exchange with $Cd^{2+}$ instead produced CdS–$Cu_{1.8}S$ Janus spheres. In Figure 2, the drawings for the sandwich and Janus spheres show that the extent of exchange, for these cation exchange reactions carried out using an excess of metal cation reagents, depends on the reaction time. Reaction time therefore controls the extent of partial cation exchange. The drawings in Figure 2 also imply different apparent orientations for the ZnS/$Cu_{1.8}S$ *vs* CdS/$Cu_{1.8}S$ particles. The ZnS–$Cu_{1.8}S$–ZnS sandwich spheres are oriented such that their interfaces are horizontal relative to the page, while for the CdS–$Cu_{1.8}S$ Janus spheres, the interfaces are oriented vertically. These differences in orientation are not random or coincidental. They correlate with crystallographic differences that result in control over the direction of cation exchange.[2]

Understanding how the direction of cation exchange correlates with crystal structure requires thinking more about the cation exchange process and taking a closer look at the crystal structures of roxbyite and wurtzite, which is the structure adopted by all of our cation exchange products. Figure 3 shows a small roxbyite nanoparticle as a single crystal, aligned in a direction where the sulfur anions form vertical planes with the copper cations between them. When a fraction of the $Cu^{+}$ cations in roxbyite is replaced with $Cd^{2+}$, there is now $Cd^{2+}$ within the crystal. CdS and $Cu_{1.8}S$ are immiscible, so they want to remain as separate phases. However, they are co-located within the same crystal, so to achieve phase separation, one or more interfaces must form between them. Interfaces are inherently high in energy, so the number of interfaces will be minimized. Additionally, interfacial energy will be minimized by aligning the crystal planes having the closest-matching interatomic spacings.

The pseudohexagonal unit cell of roxbyite $Cu_{1.8}S$ (Figure 3) has lattice constants (which correlate with sulfur-sulfur spacings) of $a$ = 3.87 Å and $c$ = 6.71 Å.[53] CdS, which has an analogous hexagonal unit cell and closely related sulfur sublattice structure (Figure 3), has lattice constants of $a$ = 4.13 Å and $c$ = 6.72 Å.[54] CdS and $Cu_{1.8}S$ minimize interfacial energy by aligning along their $c$-axis directions, as shown in Figure 3.[1] $Zn^{2+}$ is smaller than $Cd^{2+}$, and the lattice constants for ZnS ($a$ = 3.81 Å and $c$ = 6.23 Å) are smaller than for CdS.[54] ZnS and $Cu_{1.8}S$ therefore minimize interfacial energy by aligning along their $a$-axis directions ($a_{ZnS}$ = 3.81 Å, $a_{Cu1.8S(hex)}$ = 3.87 Å).[1] This means that in a single-crystal nanoparticle, the CdS and ZnS segments formed through partial cation exchange will form interfaces with $Cu_{1.8}S$ that are perpendicular to one another, as shown in Figure 3.

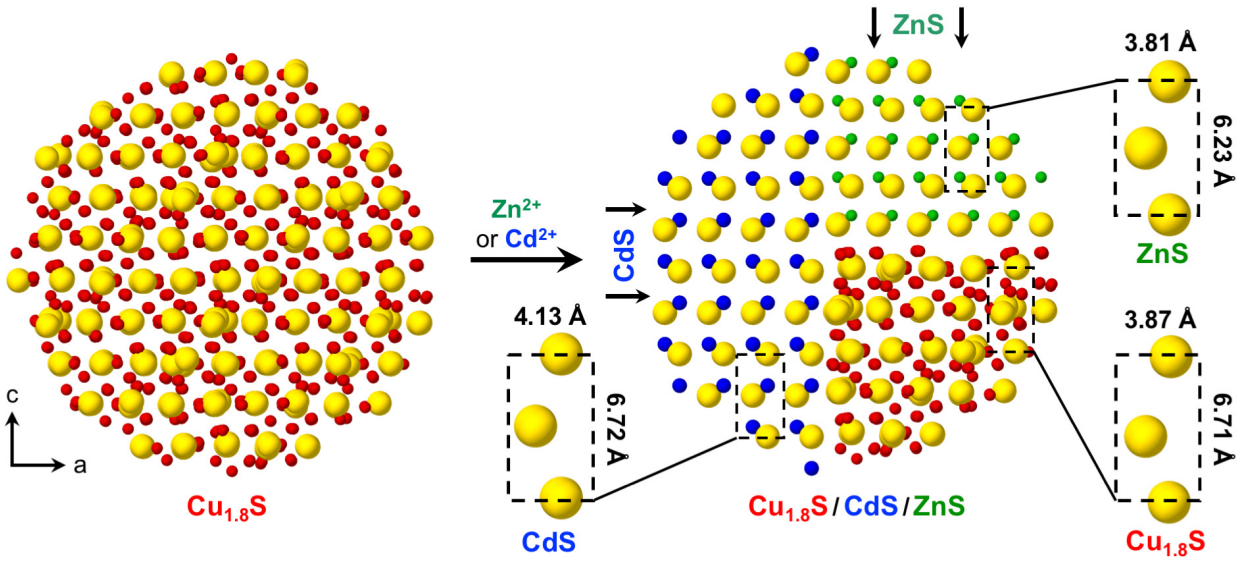


**Figure 3.** (Left) Crystal structure ([001] projection) of a roxbyite $Cu_{1.8}S$ cluster. The axis label corresponds to the a and c directions relative to the pseudohexagonal subcell within roxbyite $Cu_{1.8}S$. (Right) The same cluster with CdS and ZnS replacing parts of the $Cu_{1.8}S$ in the crystallographic orientations that are observed experimentally. The CdS/$Cu_{1.8}S$ and ZnS/$Cu_{1.8}S$ interfaces that form have the best lattice matching. A pseudohexagonal roxbyite cell is shown, along with comparable cells for wurtzite CdS and ZnS and the corresponding dimensions in each direction.

This crystallographic dependence to the direction of partial cation exchange has interesting implications for designing greater complexity into heterostructured nanoparticles. If we begin with the ZnS–$Cu_{1.8}S$–ZnS sandwich particles and perform a subsequent partial $Cd^{2+}$ exchange on the residual $Cu_{1.8}S$, CdS will interface with $Cu_{1.8}S$ in a direction perpendicular to the ZnS/$Cu_{1.8}S$ interface.[2] This cation exchange sequence forms ZnS–($Cu_{1.8}S$–CdS)–ZnS, which is a unique heterostructured particle having ZnS on the top and bottom with a central band that is half $Cu_{1.8}S$ and half CdS (Figure 4). If we instead begin with CdS–$Cu_{1.8}S$ Janus particles and perform a subsequent partial $Zn^{2+}$ exchange on the residual $Cu_{1.8}S$, the $Cu_{1.8}S$ hemisphere transforms to a ZnS–$Cu_{1.8}S$–ZnS half-sandwich.[1,2] This product, CdS–(ZnS–$Cu_{1.8}S$–ZnS) (Figure 4), and ZnS–($Cu_{1.8}S$–CdS)–ZnS are heterostructured nanoparticle isomers, as they contain the same materials but in different configurations.

Crystallographic regioselectivity, where crystal structure relationships define the regions where cation exchange occurs selectively, can also be applied to other morphologies of copper sulfide.[2] Starting with the striped ZnS–$Cu_{1.8}S$–ZnS–$Cu_{1.8}S$–ZnS nanorods in Figure 2, subsequent partial cation exchange with $Cd^{2+}$ inserts CdS perpendicular to the ZnS/$Cu_{1.8}S$ interfaces, forming ZnS–(CdS–$Cu_{1.8}S$)–ZnS–(CdS–$Cu_{1.8}S$)–ZnS (Figure 4). Starting instead with the CdS–$Cu_{1.8}S$ single-tip nanorods in Figure 2, subsequent partial cation exchange with $Zn^{2+}$ inserts ZnS in the same direction it appeared in the striped nanorods, forming CdS–ZnS–$Cu_{1.8}S$–ZnS (Figure 4). In this system, the initial $Cd^{2+}$ exchange deviates from the interface expected based on crystallographic relationships. Here, the increased reactivity of the nanorod tips wins out, and CdS prefers to form at the tips, with a horizontal interface, rather than along the sides, with a vertical interface.[2] This competition between various locations for cation exchange to occur provides flexibility in design and pathways to more complex products.

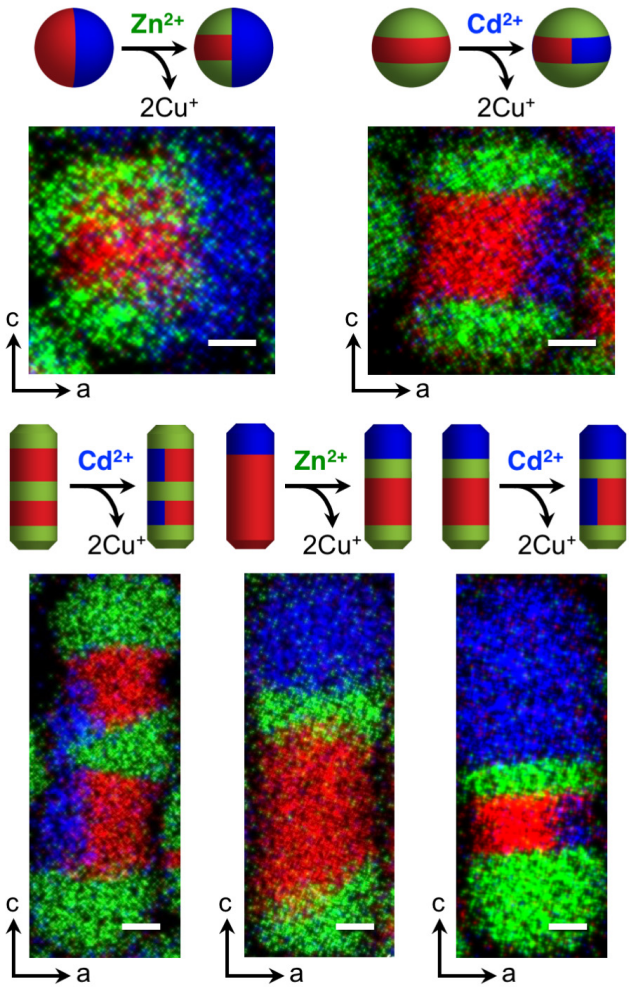


**Figure 4.** Synthetic pathways for producing complex heterostructured nanoparticle isomers of $Cu_{1.8}S$ (red), CdS (blue), and ZnS (green). Drawings represent the pathways, axes indicate the crystallographic directions, and STEM-EDS element maps are shown for each product. Scale bars are 5 nm. The STEM-EDS maps were adapted with permission from ref. 2, copyright 2018 American Chemical Society.

The concept of crystallographic regioselectivity during partial cation exchange reactions can be applied to even more complex heterostructured nanoparticles. We began by designing and synthesizing a CdS–$Cu_{1.8}S$ Janus nanorod through partial $Cd^{2+}$ cation exchange of $Cu_{1.8}S$ nanorods, with the CdS and $Cu_{1.8}S$ segments having approximately equal lengths. Next, we performed a partial $Zn^{2+}$ exchange to install ZnS stripes similar to those in Figure 2, forming CdS–ZnS–$Cu_{1.8}S$–ZnS. We then carried out a subsequent partial cation exchange with $Cd^{2+}$, anticipating that CdS would replace half of the $Cu_{1.8}S$, with an interface along the length of the nanorods (instead of perpendicular, as occurs for the ZnS/$Cu_{1.8}S$ interface). Indeed, the product that formed was CdS–ZnS–(CdS–$Cu_{1.8}S$)–ZnS (Figure 4).[2]

## 4. Heterostructured Nanorod Megalibrary

The made-to-order synthesis of CdS–ZnS–(CdS–$Cu_{1.8}S$)–ZnS heterostructured nanorods in Figure 4 confirms that we can apply multiple sequential partial cation exchange reactions to rationally design complex features into heterostructured nanorods in a predictable way based on an understanding of the reactions and the crystallographic relationships. However, this is just one example. How broadly is this approach applicable? How many sequential reactions can be applied? How precisely can the feature sizes be controlled? How complex can the heterostructured nanorods get? To answer these questions, we began by tackling an important technical issue. The partial cation exchange reactions are carried out using a significant excess of the exchanging cation.[1,2] Reaction time and/or temperature are therefore the synthetic levers available for controlling the extent of cation exchange, which are challenging to implement precisely. An alternative approach is to instead limit the extent of exchange based on stoichiometry. Here, only enough cations are introduced into solution to exchange with a desired fraction of the $Cu^+$ cations in the $Cu_{1.8}S$, and then the reaction would be allowed to go to completion.[3]

To demonstrate this alternative approach, which uses stoichiometrically-limited metal salt reagents, we performed five sequential partial cation exchange reactions on roxbyite nanorods.[3] $Cu_{1.8}S$ nanorods were injected into a mixture of oleylamine, benzyl ether, and octadecene, then precise volumes of metal salt stock solutions were sequentially injected to replace ~1/6 of the $Cu^+$ cations in each step. Injecting $Zn^{2+}$ transformed the G-1 $Cu_{1.8}S$ nanorods to G-2 ZnS–$Cu_{1.8}S$, followed by a $In^{3+}$ injection to form G-3 ZnS–$CuInS_2$–$Cu_{1.8}S$, followed by a $Ga^{3+}$ injection to form G-4 ZnS–$CuInS_2$–$CuGaS_2$–$Cu_{1.8}S$, followed by a $Co^{2+}$ injection to form G-5 ZnS–$CuInS_2$–$CuGaS_2$–CoS–$Cu_{1.8}S$, followed by a $Cd^{2+}$ injection to form G-6 ZnS–$CuInS_2$–$CuGaS_2$–CoS–(CdS–$Cu_{1.8}S$) (Figure 5). The G-6 heterostructured nanorods contain six distinct metal sulfides and six distinct types of interfaces, all within uniform colloidal rods that are approximately 20 × 55 nm. Because these nanorods are made colloidally, we can isolate tens of milligrams of product, which can be characterized by bulk methods. Powder X-ray diffraction (XRD) data for this sample corroborates the microscopy data, confirming that all six materials are present. XRD peak widths yield grain sizes that correlate well with the average segment lengths determined by transmission electron microscopy (TEM), and preferred orientation features for each material further connect the XRD data to the nanorod morphology and its constituent segments.[3]

From these studies, two important design guidelines emerge.[3] First, the order in which the metal salt exchange solutions are injected defines the sequence of materials in the heterostructured nanorods. Each new metal sulfide material that is installed in the nanorod locates at the interface between the remaining $Cu_{1.8}S$ and the material installed in the previous exchange step. This interface is observed to be poorly crystalline and defect-rich (Figure 5), and therefore may facilitate enhanced diffusion and preferential exchange in this region. Second, the orientations of the interfaces are defined by their lattice matching, which is a proxy for interfacial strain. This guideline builds on what was described above and in Figure 3, here expanding it to different materials and interface angles.

With these guidelines and capabilities in hand, we sought to answer the other questions posed above about expanding the scope and complexity of partial cation exchange reactions. Going back to Figure 5, the G-6 system began with single-tip ZnS–$Cu_{1.8}S$ nanorods. By changing the reaction conditions during the partial cation exchange reaction that formed ZnS–$Cu_{1.8}S$, two other variants could be generated: central-band $Cu_{1.8}S$–ZnS–$Cu_{1.8}S$ and double-tip ZnS–$Cu_{1.8}S$–ZnS.[3] We could also identify intermediate reaction conditions that produced a sample

containing all three G-2 ZnS/$Cu_{1.8}S$ nanorods, as well as several other ZnS/$Cu_{1.8}S$ heterostructured nanorods. Normally the formation of a mixed-population sample is viewed negatively, but here, it was done purposely because it provided a platform to scan a larger number of systems using a minimal number of samples and reactions. Starting with the mixed-population sample containing G-2 ZnS–$Cu_{1.8}S$, $Cu_{1.8}S$–ZnS–$Cu_{1.8}S$, and ZnS–$Cu_{1.8}S$–ZnS, one subsequent reaction with a different cation produced a sample containing all possible G-3 products derived from these three precursors and the exchanged cation. This mixed-population G-3 product then became the precursor for a subsequent cation exchange reaction to identify all G-4 derivatives, and so on through G-8.

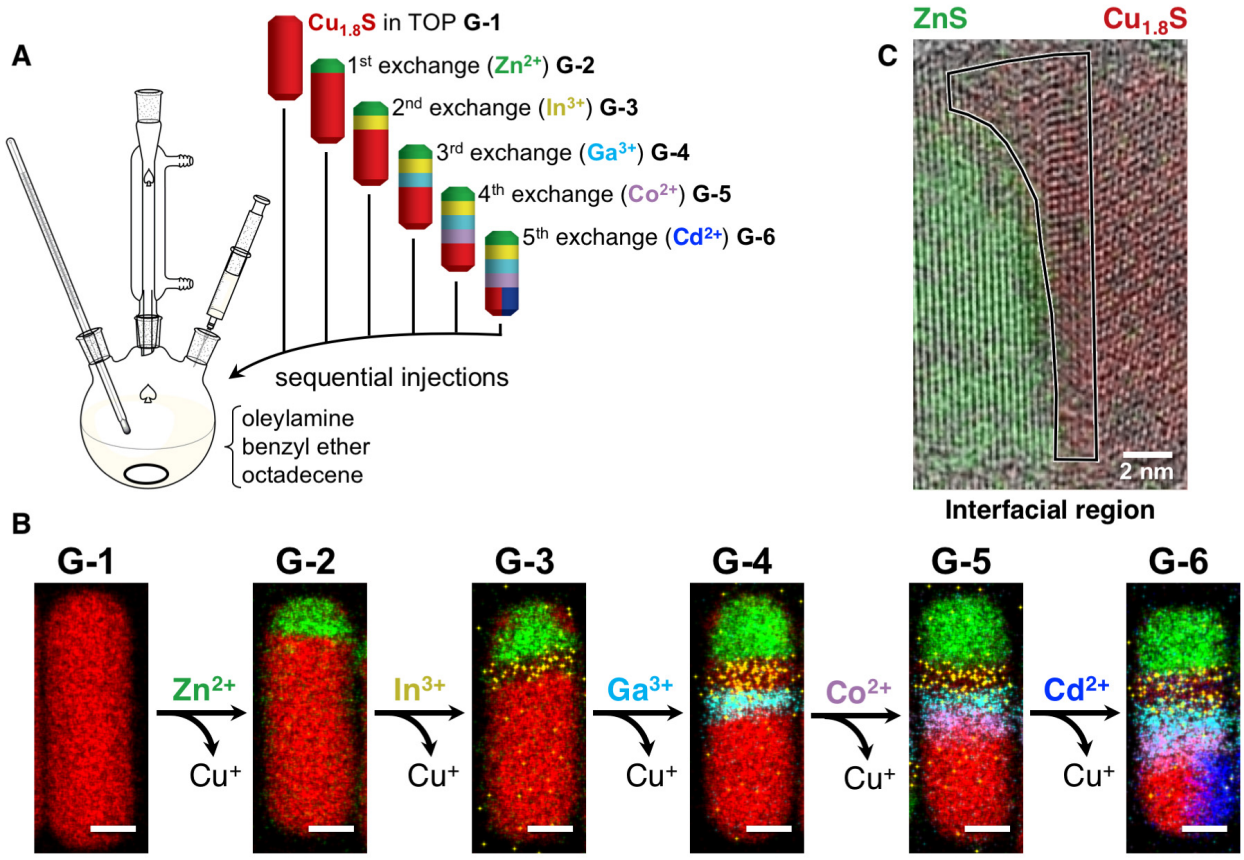


**Figure 5.** (A) Setup and general procedure for transforming G-1 $Cu_{1.8}S$ nanorods into G-6 ZnS–$CuInS_2$–$CuGaS_2$–CoS–(CdS–$Cu_{1.8}S$) heterostructured nanorods using several sequential partial cation exchange reactions. (B) STEM-EDS element maps for each nanorod. Scale bars are 10 nm. (C) HRTEM image with overlaid EDS map highlighting the interfacial region between ZnS and $Cu_{1.8}S$, which shows poor crystallinity and a higher density of defects. Adapted with permission from ref. 3, copyright 2020 American Association for the Advancement of Science.

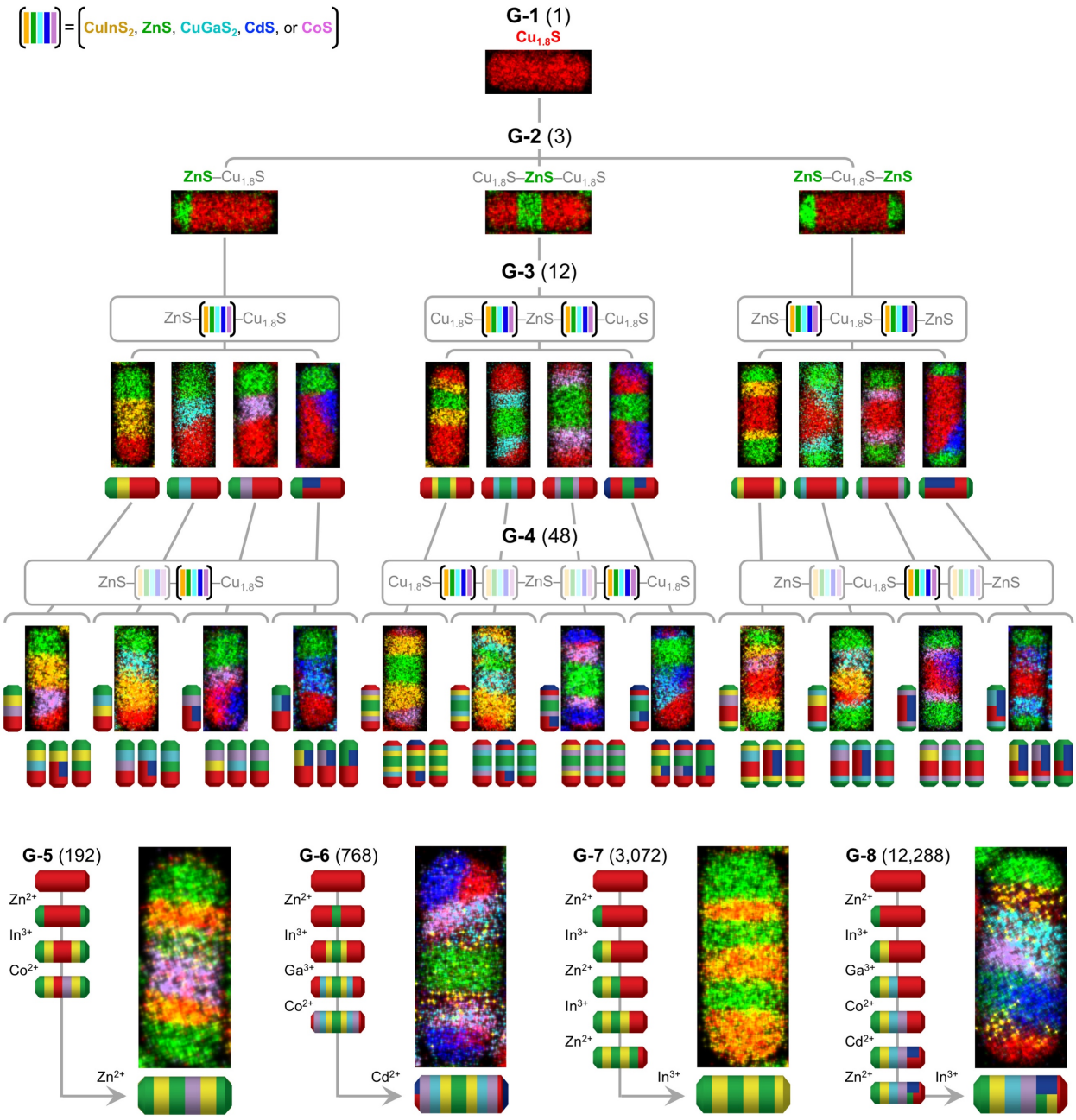


**Figure 6.** Flow chart showing how three distinct types of G-2 ZnS/$Cu_{1.8}S$ nanorods can transform into 16,380 distinct G-3 through G-8 nanorods by applying all possible sequences of partial cation exchange reactions with $Zn^{2+}$, $In^{3+}$, $Ga^{3+}$, $Co^{2+}$, and/or $Cd^{2+}$; each nanorod can transform into four derivatives using each of the four cations not used in the previous exchange step. Drawing are shown for all possible G-3 and G-4 products, along with STEM-EDS element maps for selected nanorods. One example each, along with the pathway used to synthesize it, is shown for G-5, G-6, G-7, and G-8. All nanorods are approx. 20 × 55 nm, and the key shows the materials corresponding to each color. Reproduced with permission from ref. 3, copyright 2020 American Association for the Advancement of Science.

We considered series of sequential partial exchange reactions of the mixed-population ZnS/$Cu_{1.8}S$ nanorod sample and five cations: $Zn^{2+}$, $Cd^{2+}$, $Co^{2+}$, $In^{3+}$, and $Ga^{3+}$ (Figure 6).[3] To explore the possible G-3 derivatives, we focused on the four cations not used in the previous step, i.e. $Cd^{2+}$, $Co^{2+}$, $In^{3+}$, and $Ga^{3+}$ for the ZnS/$Cu_{1.8}S$ nanorods. We then carried out four reactions. The first reaction involved partial exchange of the mixed-population ZnS/$Cu_{1.8}S$ sample with $In^{3+}$. We observed that G-2 ZnS–$Cu_{1.8}S$ formed G-3 ZnS–$CuInS_2$–$Cu_{1.8}S$, G-2 $Cu_{1.8}S$–ZnS–$Cu_{1.8}S$ formed G-3 $Cu_{1.8}S$–$CuInS_2$–ZnS–$CuInS_2$–$Cu_{1.8}S$, and G-2 ZnS–$Cu_{1.8}S$–ZnS formed G-3 ZnS–$CuInS_2$–$Cu_{1.8}S$–$CuInS_2$–ZnS. Consistent with the guidelines, the product of $In^{3+}$ exchange, $CuInS_2$, inserted between the residual $Cu_{1.8}S$ and the previous exchange product, ZnS, and formed a $CuInS_2$–$Cu_{1.8}S$ interface that minimized lattice mismatch. For the single-tip ZnS–$Cu_{1.8}S$ nanorod, this behavior mirrored that shown in Figure 5, where the new material "stepped down" the nanorod. For the central-band $Cu_{1.8}S$–ZnS–$Cu_{1.8}S$ nanorod, there were two ZnS/$Cu_{1.8}S$ interfaces. $CuInS_2$ inserted into both interfaces, and therefore "stepped outward" in both directions of the nanorod. For the double-tip ZnS–$Cu_{1.8}S$–ZnS nanorod, there also were two ZnS/$Cu_{1.8}S$ interfaces, and again $CuInS_2$ inserted into both. Here, based on their locations, the $CuInS_2$ "stepped inward" in both directions of the nanorod.

Each G-2 ZnS/$Cu_{1.8}S$ nanorod produced a derivative G-3 ZnS/$CuInS_2$/$Cu_{1.8}S$ nanorod upon partial $In^{3+}$ exchange. Similar results were obtained for the exchanges with $Ga^{3+}$, $Co^{2+}$, and $Cd^{2+}$ (Figure 6).[3] Together, the three G-2 ZnS/$Cu_{1.8}S$ nanorods could be transformed to 12 distinct G-3 nanorods through exchange with four distinct cations. Applying this same reaction strategy to the 12 G-3 nanorods – i.e. carrying out partial exchange reactions on each G-3 nanorod with the four cations not used in the previous exchange – produced 48 G-4 nanorods. These 48 G-4 nanorods transform to 192 G-5 nanorods, 768 G-6 nanorods, 3072 G-7 nanorods, and 12,288 G-8 nanorods. Synthetically feasible pathways therefore exist for transforming the three G-2 ZnS/$Cu_{1.8}S$ nanorods into 12,288 distinct G-8 derivatives.[3] Simple, rational chemistry yields isolatable quantities of uniform colloidal heterostructured nanorods having unprecedented complexity.

Each branch of the reaction scheme in Figure 6, i.e. each set of reaction pathways that emerges from a single G-2 nanorod, represents synthetically feasible routes to 5,460 derivative G-3 through G-8 nanorods. For the three available types of G-2 ZnS/$Cu_{1.8}S$ nanorods, $5{,}460 \times 3 = 12{,}288$ derivatives are potentially accessible, which is the scope of systems represented in Figure 6. However, it is possible to make other G-2 nanorods by starting the sequence with cations other than $Zn^{2+}$. As of now, we can make a total of 12 distinct G-2 nanorods in high yield: three ZnS/$Cu_{1.8}S$, three $CuGaS_2$/$Cu_{1.8}S$, and two each of $CuInS_2$/$Cu_{1.8}S$, CoS/$Cu_{1.8}S$, and CdS/$Cu_{1.8}S$ (Figure 7).[3] In principle, each of these 12 G-2 nanorods could be the starting point for a "branch," leading to a total of $5{,}460 \times 12 = 65{,}520$ distinct heterostructured nanorods containing various combinations of $Cu_{1.8}S$, ZnS, CdS, CoS, $CuInS_2$, and/or $CuGaS_2$ (Figure 7). While more than 100 members of this heterostructured nanorod megalibrary have been experimentally observed in mixed-population samples,[3] in principle it should be possible to make any of them in high yield and in isolatable quantities. To demonstrate feasibility, three samples were synthesized in ~10-40 mg batches: G-4 ZnS–$CuInS_2$–CoS–$Cu_{1.8}S$, G-6 ZnS–$CuInS_2$–$CuGaS_2$–CoS–(CdS–$Cu_{1.8}S$), and G-7 ZnS–$CuInS_2$– ZnS–$CuInS_2$– ZnS–$CuInS_2$.

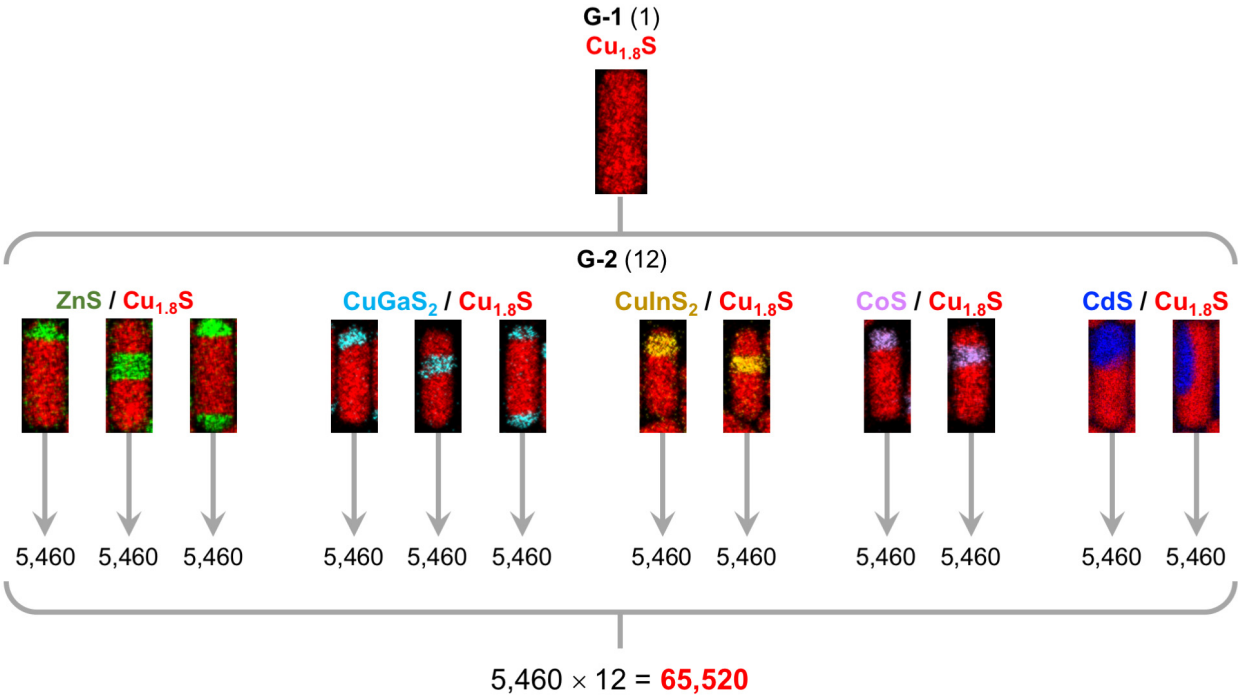


**Figure 7.** STEM-EDS element maps for each of the synthetically accessible G-2 nanorods. Each nanorod can transform to 5,460 distinct G-3 through G-8 products, as outlined in Figure 6. All together, synthetically feasible pathways exist to transform $Cu_{1.8}S$ nanorods into a megalibrary of 65,520 distinct heterostructured nanorods. The STEM-EDS maps were adapted with permission from ref. 3, copyright 2020 American Association for the Advancement of Science.

Further morphological complexity can be introduced by selectively dissolving any residual $Cu_{1.8}S$ by reacting it with trioctylphosphine (TOP) under oxidizing conditions.[1,55,56] Chemical etching of $Cu_{1.8}S$ using TOP is a multistep process that requires reduction of surface $S^{-}$ to $S^{2-}$, formation of a phosphine–sulfur bond, and subsequent oxidation and dissolution of $Cu^{2+}$.[55] This process is selective for $Cu_{1.8}S$ in the presence of other metal sulfides. For example, spherical CdS–(ZnS–$Cu_{1.8}S$–ZnS) nanoparticles can be transformed to CdS–(ZnS– –ZnS) (Figure 8), where " " corresponds to the void space created after the $Cu_{1.8}S$ was dissolved.[1] Additionally, the $Cu_{1.8}S$ segments of ZnS–$Cu_{1.8}S$–ZnS–$Cu_{1.8}S$–ZnS striped nanorods can be partially etched to narrow the widths of each $Cu_{1.8}S$ segment (Figure 8).[1] Exchanging the remaining $Cu^{+}$ with $Zn^{2+}$ converts the entire nanorod to ZnS while preserving the intricate sculpted morphology (Figure 8).[1]

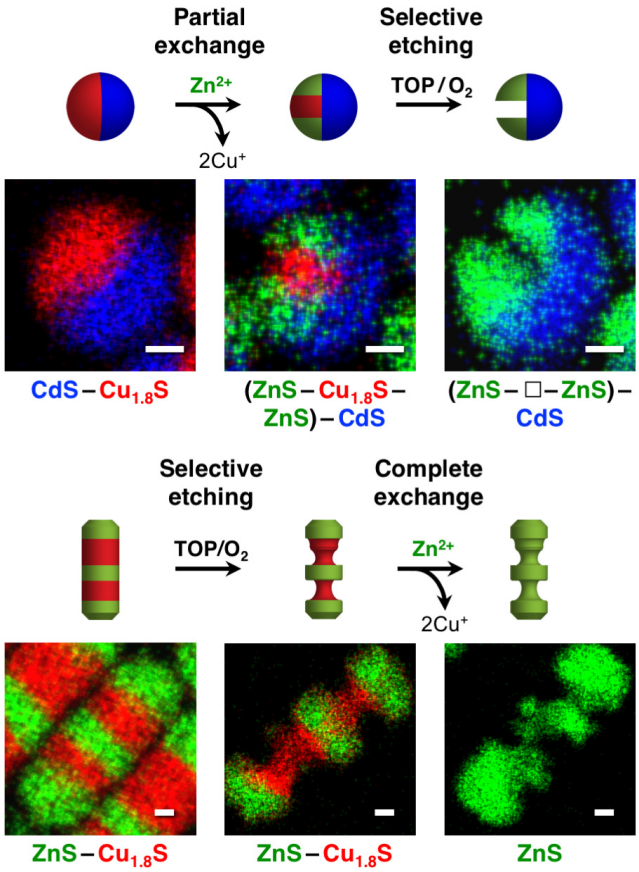


**Figure 8.** Drawings and STEM-EDS element maps highlighting synthetic pathways to etched and sculpted heterostructured nanoparticles by combining partial sequential cation exchange and selective chemical etching of $Cu_{1.8}S$. Scale bars are 5 nm. Red = $Cu_{1.8}S$, blue = CdS, green = ZnS. The STEM-EDS maps were adapted with permission from ref. 1, copyright 2018 American Association for the Advancement of Science.

## 5. Applying Design Guidelines to Complex Targets

We now return to the example used to motivate this work – a water splitting construct containing a central light-absorbing semiconductor with different catalysts on opposite ends. As a simplified model system (since chemistry is not yet available to deposit the most desired materials for this application), we consider a spherical CdS nanoparticle having one metal that is a known reduction catalyst (i.e. Pt) deposited on one side and another metal that is a known oxidation catalyst (i.e. Au) deposited on the other.[57] While some seeded growth methods are capable of forming hybrid nanoparticles,[8–11] the Au–CdS–Pt system is out of reach based on current knowledge and capabilities. Control experiments confirm that Pt and Au both deposit as small particles all over the CdS surface.[1] Sequential seeded growth reactions also result in Pt and Au decorating the entire surface, without significant spatial separation.[1] Approaching this retrosynthetically,[1] we can consider starting with spherical particles of $Cu_{1.8}S$ and using partial exchange with $Cd^{2+}$ to form CdS–$Cu_{1.8}S$ (Figure 9). This reaction is used to break the symmetry of the sphere to produce a Janus particle. We can exploit the different surface chemistry of CdS vs $Cu_{1.8}S$ to selectively deposit Pt on $Cu_{1.8}S$ to form CdS–$Cu_{1.8}S$–Pt (Figure 9). We can then complete the exchange of the remaining $Cu^{+}$ with $Cd^{2+}$ to completely convert the CdS–$Cu_{1.8}S$

particle to CdS, resulting in a spherical CdS particle with Pt on one side. Subsequent seeded growth of Au targets the bare CdS surface, forming Au–CdS–Pt (Figure 9). This demonstrates, for a model system, how partial cation exchange can be used to program asymmetry and interfaces while other methods, such as seeded growth, can be used in tandem to target otherwise inaccessible constructs that are mimics of high-value functional targets.

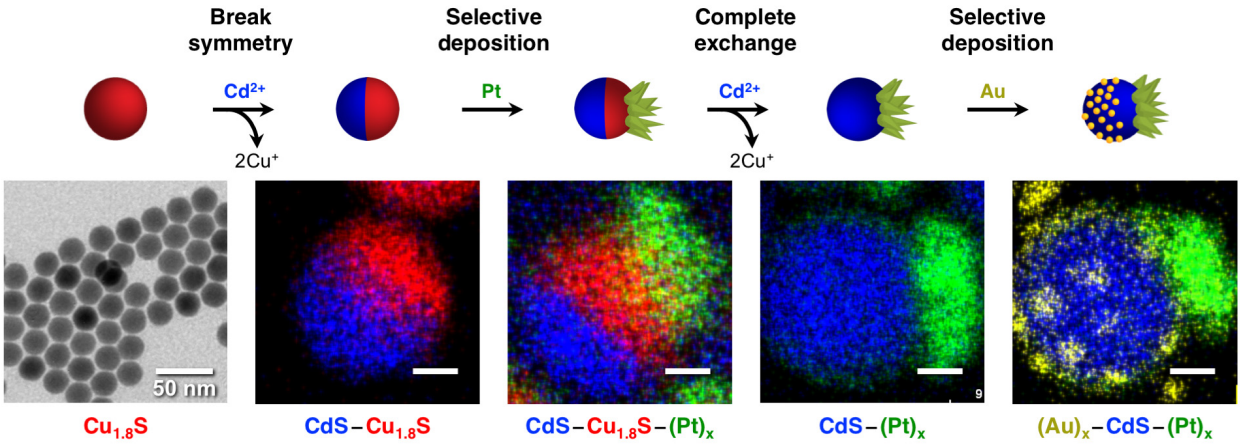


**Figure 9.** Drawings and STEM-EDS element maps highlighting synthetic pathways to asymmetric metal–semiconductor–metal heterostructured nanoparticles, $(Au)_x$–CdS–$(Pt)_x$, by combining partial sequential cation exchange and regioselective seeded growth. Unless otherwise noted, scale bars are 5 nm. Red = $Cu_{1.8}S$, blue = CdS, green = ZnS, yellow = Au. The STEM-EDS maps were adapted with permission from ref. 1, copyright 2018 American Association for the Advancement of Science.

The system described above is just one example of how the design guidelines that are emerging for sequential partial cation exchange reactions, and more generally for postsynthetic nanoparticle modification, are beginning to enable the made-to-order synthesis of targeted heterostructured nanoparticles with increasing levels of complexity.

## 6. Conclusions and Outlook

We are approaching a point where computational methods are able to predict an incomprehensibly large number of complex new nanostructured materials with potentially outstanding properties. We are also learning more and more about the properties of materials, by themselves and interfaced together, that will increase our ability to design new functional nanostructures. Because of these advances in prediction capabilities, synthesis is quickly becoming the bottleneck, and experimental realization lags behind design. Nanosynthetic chemistry remains far more limited in scope than molecular chemistry, where a more sophisticated reaction toolbox and greater mechanistic understanding of reactions is available. How does a nanosynthetic chemist keep pace with the frequency and scope of predictions so that complex nanostructured materials can be made in the laboratory efficiently, in large quantities, with high purities and yields, and in the shortest time possible? Postsynthetic modification strategies such as sequential partial cation exchange begin to make this possible, even if only for a limited number of model systems at this stage. They allow the synthesis of complex nanostructures to be approached retrosynthetically, in a made-to-order manner.

While sequential partial cation exchange reactions now provide access to a megalibrary of complex heterostructured metal sulfide nanoparticles, these are largely model systems used to demonstrate concepts and possibilities, not products targeted for their properties. Applying these design guidelines to functional heterostructures will begin to advance the application areas that motivated this work. We have limited ourselves to just 8 metal sulfide materials – $Cu_{1.8}S$, ZnS, CdS, CoS, MnS, $Ni_9S_8$, $CuInS_2$, and $CuGaS_2$ – and have shown that specific segmentation patterns, controlled segment sizes, and scalability are possible. Various combinations of these materials in heterostructured nanoparticles could achieve long-lived charge separation, emission or absorption of specific wavelengths of light, and photocatalytic activity. Other cations in metal sulfide nanoparticles,[37] and other classes of nanoparticles, including selenides,[40,47] tellurides,[58] phosphides,[59] and halides,[60,61] are amenable to ion exchange, providing potential avenues to expanding the scope of materials and properties. Most cation exchange capabilities exist for sulfides, however, so expanding to other materials will require expanding the scope of cation exchange reactions. Finally, not all of the heterostructured nanoparticles observed experimentally can be rationalized based on established design guidelines. Additional factors must be identified and considered to fully realize made-to-order synthesis.

## BIOGRAPHIES

**Benjamin C. Steimle** received his B.S. in chemistry from the State University of New York at New Paltz. He is currently pursuing a Ph.D. at Penn State under the supervision of Raymond E. Schaak studying post-synthetic modification of colloidal nanoparticles and developing syntheses for complex heterostructured nanoparticles.

**Julie L. Fenton** received her B.S. in chemistry from Messiah College and her Ph.D. in chemistry from Penn State under the supervision of Raymond E. Schaak, focused on synthetic method development for inorganic nanomaterials. She is currently an Arnold O. Beckman Postdoctoral Fellow in the group of William R. Dichtel at Northwestern University, researching crystalline organic materials and their applications.

**Raymond E. Schaak** received his B.S. in chemistry from Lebanon Valley College and his Ph.D. in chemistry from Penn State. After a postdoc at Princeton, he joined the chemistry faculty at Texas A&M. He is currently the DuPont Professor of Materials Chemistry at Penn State and has a courtesy appointment in Chemical Engineering. His research interests focus on synthetic inorganic nanochemistry, solid-state chemistry, and new materials discovery.

## ACKNOWLEDGMENTS

This work was supported by the U.S. National Science Foundation under grant DMR-1904122.

## REFERENCES

1. Fenton, J. L.; Steimle, B. C.; Schaak, R. E. Tunable Intraparticle Frameworks for Creating Complex Heterostructured Nanoparticle Libraries. *Science* **2018**, *360*, 513–517. https://doi.org/10.1126/science.aar5597.

2. Fenton, J. L.; Steimle, B.; Schaak, R. E. Exploiting Crystallographic Regioselectivity to Engineer Asymmetric Three-Component Colloidal Nanoparticle Isomers Using Partial Cation Exchange Reactions. *J. Am. Chem. Soc.* **2018**, *140*, 6771–6775. https://doi.org/10.1021/jacs.8b03338.
3. Steimle, B. C.; Fenton, J. L.; Schaak, R. E. Rational Construction of a Scalable Heterostructured Nanorod Megalibrary. *Science* **2020**, *367*, 418–424. https://doi.org/10.1126/science.aaz1172.
4. Kim, T.-H.; Cho, K.-S.; Lee, E. K.; Lee, S. J.; Chae, J.; Kim, J. W.; Kim, D. H.; Kwon, J.-Y.; Amaratunga, G.; Lee, S. Y.; Choi, B. L.; Kuk, Y.; Kim, J. M.; Kim, K. Full-Colour Quantum Dot Displays Fabricated by Transfer Printing. *Nature Photon.* **2011**, *5*, 176–182. https://doi.org/10.1038/nphoton.2011.12.
5. O'Neal, D. P.; Hirsch, L. R.; Halas, N. J.; Payne, J. D.; West, J. L. Photo-Thermal Tumor Ablation in Mice Using near Infrared-Absorbing Nanoparticles. *Cancer Letters* **2004**, *209*, 171–176. https://doi.org/10.1016/j.canlet.2004.02.004.
6. Jaque, D.; Maestro, L. M.; del Rosal, B.; Haro-Gonzalez, P.; Benayas, A.; Plaza, J. L.; Rodríguez, E. M.; Solé, J. G. Nanoparticles for Photothermal Therapies. *Nanoscale* **2014**, *6*, 9494–9530. https://doi.org/10.1039/C4NR00708E.
7. Choi, J.-H.; Wang, H.; Oh, S. J.; Paik, T.; Sung, P.; Sung, J.; Ye, X.; Zhao, T.; Diroll, B. T.; Murray, C. B.; Kagan, C. R. Exploiting the Colloidal Nanocrystal Library to Construct Electronic Devices. *Science* **2016**, *352*, 205–208. https://doi.org/10.1126/science.aad0371.
8. Buck, M. R.; Bondi, J. F.; Schaak, R. E. A Total-Synthesis Framework for the Construction of High-Order Colloidal Hybrid Nanoparticles. *Nature Chem.* **2012**, *4*, 37–44. https://doi.org/10.1038/nchem.1195.
9. Hodges, J. M.; Schaak, R. E. Controlling Configurational Isomerism in Three-Component Colloidal Hybrid Nanoparticles. *Acc. Chem. Res.* **2017**, *50*, 1433–1440. https://doi.org/10.1021/acs.accounts.7b00105.
10. Shi, W.; Zeng, H.; Sahoo, Y.; Ohulchanskyy, T. Y.; Ding, Y.; Wang, Z. L.; Swihart, M.; Prasad, P. N. A General Approach to Binary and Ternary Hybrid Nanocrystals. *Nano Lett.* **2006**, *6*, 875–881. https://doi.org/10.1021/nl0600833.
11. Costi, R.; Saunders, A. E.; Banin, U. Colloidal Hybrid Nanostructures: A New Type of Functional Materials. *Angew. Chem. Int. Ed.* **2010**, *49*, 4878–4897. https://doi.org/10.1002/anie.200906010.
12. Razgoniaeva, N.; Moroz, P.; Lambright, S.; Zamkov, M. Photocatalytic Applications of Colloidal Heterostructured Nanocrystals: What's Next? *J. Phys. Chem. Lett.* **2015**, *6*, 4352–4359. https://doi.org/10.1021/acs.jpclett.5b01883.
13. Meekins, B. H.; Kamat, P. V. Role of Water Oxidation Catalyst $IrO_2$ in Shuttling Photogenerated Holes Across $TiO_2$ Interface. *J. Phys. Chem. Lett.* **2011**, *2*, 2304–2310. https://doi.org/10.1021/jz200852m.
14. Kalisman, P.; Nakibli, Y.; Amirav, L. Perfect Photon-to-Hydrogen Conversion Efficiency. *Nano Lett.* **2016**, *16*, 1776–1781. https://doi.org/10.1021/acs.nanolett.5b04813.
15. Xie, J.; Zhang, F.; Aronova, M.; Zhu, L.; Lin, X.; Quan, Q.; Liu, G.; Zhang, G.; Choi, K.-Y.; Kim, K.; Sun, X.; Lee, S.; Sun, S.; Leapman, R.; Chen, X. Manipulating the Power of an Additional Phase: A Flower-like Au−$Fe_3O_4$ Optical Nanosensor for Imaging Protease Expressions In Vivo. *ACS Nano* **2011**, *5*, 3043–3051. https://doi.org/10.1021/nn200161v.

16. Banin, U.; Ben-Shahar, Y.; Vinokurov, K. Hybrid Semiconductor–Metal Nanoparticles: From Architecture to Function. *Chem. Mater.* **2014**, *26*, 97–110. https://doi.org/10.1021/cm402131n.
17. Oh, N.; Kim, B. H.; Cho, S.-Y.; Nam, S.; Rogers, S. P.; Jiang, Y.; Flanagan, J. C.; Zhai, Y.; Kim, J.-H.; Lee, J.; Yu, Y.; Cho, Y. K.; Hur, G.; Zhang, J.; Trefonas, P.; Rogers, J. A.; Shim, M. Double-Heterojunction Nanorod Light-Responsive LEDs for Display Applications. *Science* **2017**, *355*, 616–619. https://doi.org/10.1126/science.aal2038.
18. Wang, H.; Pumera, M. Fabrication of Micro/Nanoscale Motors. *Chem. Rev.* **2015**, *115*, 8704–8735. https://doi.org/10.1021/acs.chemrev.5b00047.
19. Wang, W.; Duan, W.; Ahmed, S.; Sen, A.; Mallouk, T. E. From One to Many: Dynamic Assembly and Collective Behavior of Self-Propelled Colloidal Motors. *Acc. Chem. Res.* **2015**, *48*, 1938–1946. https://doi.org/10.1021/acs.accounts.5b00025.
20. Burda, C.; Chen, X.; Narayanan, R.; El-Sayed, M. A. Chemistry and Properties of Nanocrystals of Different Shapes. *Chem. Rev.* **2005**, *105*, 1025–1102. https://doi.org/10.1021/cr030063a.
21. Wang, Y.; He, J.; Liu, C.; Chong, W. H.; Chen, H. Thermodynamics versus Kinetics in Nanosynthesis. *Angew. Chem. Int. Ed.* **2015**, *54*, 2022–2051. https://doi.org/10.1002/anie.201402986.
22. Yin, Y.; Alivisatos, A. P. Colloidal Nanocrystal Synthesis and the Organic–Inorganic Interface. *Nature* **2005**, *437*, 664–670. https://doi.org/10.1038/nature04165.
23. Hühn, J.; Carrillo-Carrion, C.; Soliman, M. G.; Pfeiffer, C.; Valdeperez, D.; Masood, A.; Chakraborty, I.; Zhu, L.; Gallego, M.; Yue, Z.; Carril, M.; Feliu, N.; Escudero, A.; Alkilany, A. M.; Pelaz, B.; del Pino, P.; Parak, W. J. Selected Standard Protocols for the Synthesis, Phase Transfer, and Characterization of Inorganic Colloidal Nanoparticles. *Chem. Mater.* **2017**, *29*, 399–461. https://doi.org/10.1021/acs.chemmater.6b04738.
24. Xia, Y.; Xiong, Y.; Lim, B.; Skrabalak, S. E. Shape-Controlled Synthesis of Metal Nanocrystals: Simple Chemistry Meets Complex Physics? *Angew. Chem. Int. Ed.* **2009**, *48*, 60–103. https://doi.org/10.1002/anie.200802248.
25. Xia, Y.; Xia, X.; Peng, H.-C. Shape-Controlled Synthesis of Colloidal Metal Nanocrystals: Thermodynamic versus Kinetic Products. *J. Am. Chem. Soc.* **2015**, *137*, 7947–7966. https://doi.org/10.1021/jacs.5b04641.
26. Polavarapu, L.; Mourdikoudis, S.; Pastoriza-Santos, I.; Pérez-Juste, J. Nanocrystal Engineering of Noble Metals and Metal Chalcogenides: Controlling the Morphology, Composition and Crystallinity. *CrystEngComm* **2015**, *17*, 3727–3762. https://doi.org/10.1039/C5CE00112A.
27. Weiner, R. G.; Kunz, M. R.; Skrabalak, S. E. Seeding a New Kind of Garden: Synthesis of Architecturally Defined Multimetallic Nanostructures by Seed-Mediated Co-Reduction. *Acc. Chem. Res.* **2015**, *48*, 2688–2695. https://doi.org/10.1021/acs.accounts.5b00300.
28. Gilroy, K. D.; Ruditskiy, A.; Peng, H.-C.; Qin, D.; Xia, Y. Bimetallic Nanocrystals: Syntheses, Properties, and Applications. *Chem. Rev.* **2016**, *116*, 10414–10472. https://doi.org/10.1021/acs.chemrev.6b00211.
29. Mark, A. G.; Gibbs, J. G.; Lee, T.-C.; Fischer, P. Hybrid Nanocolloids with Programmed Three-Dimensional Shape and Material Composition. *Nature Mater.* **2013**, *12*, 802–807. https://doi.org/10.1038/nmat3685.
30. Nicewarner-Peña, S. R.; Freeman, R. G.; Reiss, B. D.; He, L.; Peña, D. J.; Walton, I. D.; Cromer, R.; Keating, C. D.; Natan, M. J. Submicrometer Metallic Barcodes. *Science* **2001**, *294*, 137–141. https://doi.org/10.1126/science.294.5540.137.

31. Chen, P.-C.; Liu, X.; Hedrick, J. L.; Xie, Z.; Wang, S.; Lin, Q.-Y.; Hersam, M. C.; Dravid, V. P.; Mirkin, C. A. Polyelemental Nanoparticle Libraries. *Science* **2016**, *352*, 1565–1569. https://doi.org/10.1126/science.aaf8402.
32. Chen, P.-C.; Liu, M.; Du, J. S.; Meckes, B.; Wang, S.; Lin, H.; Dravid, V. P.; Wolverton, C.; Mirkin, C. A. Interface and Heterostructure Design in Polyelemental Nanoparticles. *Science* **2019**, *363*, 959–964. https://doi.org/10.1126/science.aav4302.
33. Buck, M. R.; Schaak, R. E. Emerging Strategies for the Total Synthesis of Inorganic Nanostructures. *Angew. Chem. Int. Ed.* **2013**, *52*, 6154–6178. https://doi.org/10.1002/anie.201207240.
34. Anderson, B. D.; Tracy, J. B. Nanoparticle Conversion Chemistry: Kirkendall Effect, Galvanic Exchange, and Anion Exchange. *Nanoscale* **2014**, *6*, 12195–12216. https://doi.org/10.1039/C4NR02025A.
35. Hodges, J. M.; Kletetschka, K.; Fenton, J. L.; Read, C. G.; Schaak, R. E. Sequential Anion and Cation Exchange Reactions for Complete Material Transformations of Nanoparticles with Morphological Retention. *Angew. Chem. Int. Ed.* **2015**, *54*, 8669–8672. https://doi.org/10.1002/anie.201504099.
36. Xia, X.; Wang, Y.; Ruditskiy, A.; Xia, Y. 25th Anniversary Article: Galvanic Replacement: A Simple and Versatile Route to Hollow Nanostructures with Tunable and Well-Controlled Properties. *Adv. Mater.* **2013**, *25*, 6313–6333. https://doi.org/10.1002/adma.201302820.
37. De Trizio, L.; Manna, L. Forging Colloidal Nanostructures via Cation Exchange Reactions. *Chem. Rev.* **2016**, *116*, 10852–10887. https://doi.org/10.1021/acs.chemrev.5b00739.
38. Rivest, J. B.; Jain, P. K. Cation Exchange on the Nanoscale: An Emerging Technique for New Material Synthesis, Device Fabrication, and Chemical Sensing. *Chem. Soc. Rev.* **2013**, *42*, 89–96. https://doi.org/10.1039/C2CS35241A.
39. Gupta, S.; Kershaw, S. V.; Rogach, A. L. 25th Anniversary Article: Ion Exchange in Colloidal Nanocrystals. *Adv. Mater.* **2013**, *25*, 6923–6944. https://doi.org/10.1002/adma.201302400.
40. Son, D. H.; Hughes, S. M.; Yin, Y.; Alivisatos, A. P. Cation Exchange Reactions in Ionic Nanocrystals. *Science* **2004**, *306*, 1009–1012. https://doi.org/10.1126/science.1103755.
41. Fan, Z.; Lin, L.-C.; Buijs, W.; Vlugt, T. J. H.; van Huis, M. A. Atomistic Understanding of Cation Exchange in PbS Nanocrystals Using Simulations with Pseudoligands. *Nat. Commun.* **2016**, *7*, 11503. https://doi.org/10.1038/ncomms11503.
42. Gui, J.; Ji, M.; Liu, J.; Xu, M.; Zhang, J.; Zhu, H. Phosphine-Initiated Cation Exchange for Precisely Tailoring Composition and Properties of Semiconductor Nanostructures: Old Concept, New Applications. *Angewandte Chemie International Edition* **2015**, *54*, 3683–3687. https://doi.org/10.1002/anie.201410053.
43. Miszta, K.; Gariano, G.; Brescia, R.; Marras, S.; De Donato, F.; Ghosh, S.; De Trizio, L.; Manna, L. Selective Cation Exchange in the Core Region of $Cu_{2-x}Se/Cu_{2-x}S$ Core/Shell Nanocrystals. *J. Am. Chem. Soc.* **2015**, *137*, 12195–12198. https://doi.org/10.1021/jacs.5b06379.
44. Groeneveld, E.; Witteman, L.; Lefferts, M.; Ke, X.; Bals, S.; Van Tendeloo, G.; de Mello Donega, C. Tailoring ZnSe–CdSe Colloidal Quantum Dots via Cation Exchange: From Core/Shell to Alloy Nanocrystals. *ACS Nano* **2013**, *7*, 7913–7930. https://doi.org/10.1021/nn402931y.

45. Lesnyak, V.; Brescia, R.; Messina, G. C.; Manna, L. Cu Vacancies Boost Cation Exchange Reactions in Copper Selenide Nanocrystals. *J. Am. Chem. Soc.* **2015**, *137*, 9315–9323. https://doi.org/10.1021/jacs.5b03868.
46. Casavola, M.; van Huis, M. A.; Bals, S.; Lambert, K.; Hens, Z.; Vanmaekelbergh, D. Anisotropic Cation Exchange in PbSe/CdSe Core/Shell Nanocrystals of Different Geometry. *Chem. Mater.* **2012**, *24*, 294–302. https://doi.org/10.1021/cm202796s.
47. Li, H.; Zanella, M.; Genovese, A.; Povia, M.; Falqui, A.; Giannini, C.; Manna, L. Sequential Cation Exchange in Nanocrystals: Preservation of Crystal Phase and Formation of Metastable Phases. *Nano Lett.* **2011**, *11*, 4964–4970. https://doi.org/10.1021/nl202927a.
48. Luther, J. M.; Zheng, H.; Sadtler, B.; Alivisatos, A. P. Synthesis of PbS Nanorods and Other Ionic Nanocrystals of Complex Morphology by Sequential Cation Exchange Reactions. *J. Am. Chem. Soc.* **2009**, *131*, 16851–16857. https://doi.org/10.1021/ja906503w.
49. Enright, M. J.; Cossairt, B. M. Synthesis of Tailor-Made Colloidal Semiconductor Heterostructures. *Chem. Commun.* **2018**, *54*, 7109–7122. https://doi.org/10.1039/C8CC03498B.
50. Coughlan, C.; Ibáñez, M.; Dobrozhan, O.; Singh, A.; Cabot, A.; Ryan, K. M. Compound Copper Chalcogenide Nanocrystals. *Chem. Rev.* **2017**, *117*, 5865–6109. https://doi.org/10.1021/acs.chemrev.6b00376.
51. Liu, Y.; Liu, M.; Yin, D.; Qiao, L.; Fu, Z.; Swihart, M. T. Selective Cation Incorporation into Copper Sulfide Based Nanoheterostructures. *ACS Nano* **2018**, *12*, 7803–7811. https://doi.org/10.1021/acsnano.8b01871.
52. Ha, D.-H.; Caldwell, A. H.; Ward, M. J.; Honrao, S.; Mathew, K.; Hovden, R.; Koker, M. K. A.; Muller, D. A.; Hennig, R. G.; Robinson, R. D. Solid–Solid Phase Transformations Induced through Cation Exchange and Strain in 2D Heterostructured Copper Sulfide Nanocrystals. *Nano Lett.* **2014**, *14*, 7090–7099. https://doi.org/10.1021/nl5035607.
53. Powell, A. E.; Hodges, J. M.; Schaak, R. E. Preserving Both Anion and Cation Sublattice Features during a Nanocrystal Cation-Exchange Reaction: Synthesis of Metastable Wurtzite-Type CoS and MnS. *J. Am. Chem. Soc.* **2016**, *138*, 471–474. https://doi.org/10.1021/jacs.5b10624.
54. Xu, Y.-N.; Ching, W. Y. Electronic, Optical, and Structural Properties of Some Wurtzite Crystals. *Phys. Rev. B* **1993**, *48*, 4335–4351. https://doi.org/10.1103/PhysRevB.48.4335.
55. Nelson, A.; Ha, D.-H.; Robinson, R. D. Selective Etching of Copper Sulfide Nanoparticles and Heterostructures through Sulfur Abstraction: Phase Transformations and Optical Properties. *Chem. Mater.* **2016**, *28*, 8530–8541. https://doi.org/10.1021/acs.chemmater.6b02764.
56. Butterfield, A. G.; Steimle, B. C.; Schaak, R. E. Retrosynthetic Design of Morphologically Complex Metal Sulfide Nanoparticles Using Sequential Partial Cation Exchange and Chemical Etching. *ACS Materials Lett.* **2020**, *2*, 1106–1114. https://doi.org/10.1021/acsmaterialslett.0c00287.
57. Ma, L.; Chen, K.; Nan, F.; Wang, J.-H.; Yang, D.-J.; Zhou, L.; Wang, Q.-Q. Improved Hydrogen Production of Au–Pt–CdS Hetero-Nanostructures by Efficient Plasmon-Induced Multipathway Electron Transfer. *Adv. Funct. Mater.* **2016**, *26*, 6076–6083. https://doi.org/10.1002/adfm.201601651.

58. Tu, R.; Xie, Y.; Bertoni, G.; Lak, A.; Gaspari, R.; Rapallo, A.; Cavalli, A.; De Trizio, L.; Manna, L. Influence of the Ion Coordination Number on Cation Exchange Reactions with Copper Telluride Nanocrystals. *J. Am. Chem. Soc.* **2016**, *138*, 7082–7090. https://doi.org/10.1021/jacs.6b02830.
59. De Trizio, L.; Gaspari, R.; Bertoni, G.; Kriegel, I.; Moretti, L.; Scotognella, F.; Maserati, L.; Zhang, Y.; Messina, G. C.; Prato, M.; Marras, S.; Cavalli, A.; Manna, L. $Cu_{3-x}P$ Nanocrystals as a Material Platform for Near-Infrared Plasmonics and Cation Exchange Reactions. *Chem. Mater.* **2015**, *27*, 1120–1128. https://doi.org/10.1021/cm5044792.
60. Eperon, G. E.; Ginger, D. S. B-Site Metal Cation Exchange in Halide Perovskites. *ACS Energy Lett.* **2017**, *2*, 1190–1196. https://doi.org/10.1021/acsenergylett.7b00290.
61. Nedelcu, G.; Protesescu, L.; Yakunin, S.; Bodnarchuk, M. I.; Grotevent, M. J.; Kovalenko, M. V. Fast Anion-Exchange in Highly Luminescent Nanocrystals of Cesium Lead Halide Perovskites ($CsPbX_3$, X = Cl, Br, I). *Nano Lett.* **2015**, *15*, 5635–5640. https://doi.org/10.1021/acs.nanolett.5b02404.